Supporting Information

Amino Acid Functionalized Phosphorene: An Optical sensing platform for the Detection of Antibiotic Residues in Milk and a Clay Based Electrical CO_2 Sensor

Nasrin Sultana[1,2], Palash Jyoti Medhi[1,2], Neelotpal Sen Sarma[1,2*]

[1]Institute of Advanced Study in Science and Technology, Paschim Boragaon, Guwahati-35, Assam, India

[2]Academy of Scientific and Innovative Research (AcSIR), Ghaziabad-201002, India

***Corresponding author**: neelot@iasst.gov.in

Supporting Information: SI

Figure S1 shows the high-resolution XPS spectra of Ph and PhA composite for P 2p, O 1s, C 1s, and N 1s. The Shirley method was used to correct the background of the spectra. Figure S1(a & b) shows the XPS spectra of Ph for P 2p, O 1s. Ph shows two doublets at 133.13 and 133.98 eV corresponding to $2p_{1/2}$ and $2p_{3/2}$ respectively. Along with it, a sub-band is also observed at 134.82 eV which is related to the $(PO)_x$. This arises due to the partial oxidation of the exfoliated phosphorene nanosheets. We have also encountered two peaks for 1s oxygen binding energy at 532.28 and 532.76 corresponding to P-OH and P=O respectively.

We have also analyzed the XPS spectra of PhA as shown in Figure S1(c to f). Figure S1(c) implies the XPS spectra of P 2p, which corresponds to three characteristic peaks at 132.52 eV, 133.49 eV, and 134.31 eV for $2p_{1/2}$, $2p_{3/2}$, and $(PO)_x$ respectively. This $(PO)_x$ sub band is observed just like the pristine Ph. Figure S1(d) shows the spectra of O 1s which have two characteristic peaks at 531.49 eV and 532.5 eV for P-OH and P=O respectively. Figure S1(e) shows the 1s binding energy of carbon in the case of PhA. The spectra are fitted with four components based on the chemical structure of arginine. The characteristic peaks at 284.64, 284.94, 285.82, and 287.86 eV imply C-N, C-C/C-H, HN=C-NH/HN=C-NH_2, and O=C-OH bond respectively. Along with it, we have also analyzed the 1s binding energy of nitrogen which also shows four characteristics at 399.73, 400.74, 400.17, and 398.67 eV corresponding to –NH_2, -NH, P-N, P-N-C respectively (Figure S1(f)). However, after treating with Arg the peaks correspond to $2p_{3/2}$, $2p_{1/2}$, and (PO)x shifts its position by 3.08, 2.93, and 0.38 eV. This indicates that there is an extraction of electrons from Arg taking place which will enrich the electron density of the composite i.e., PhA.

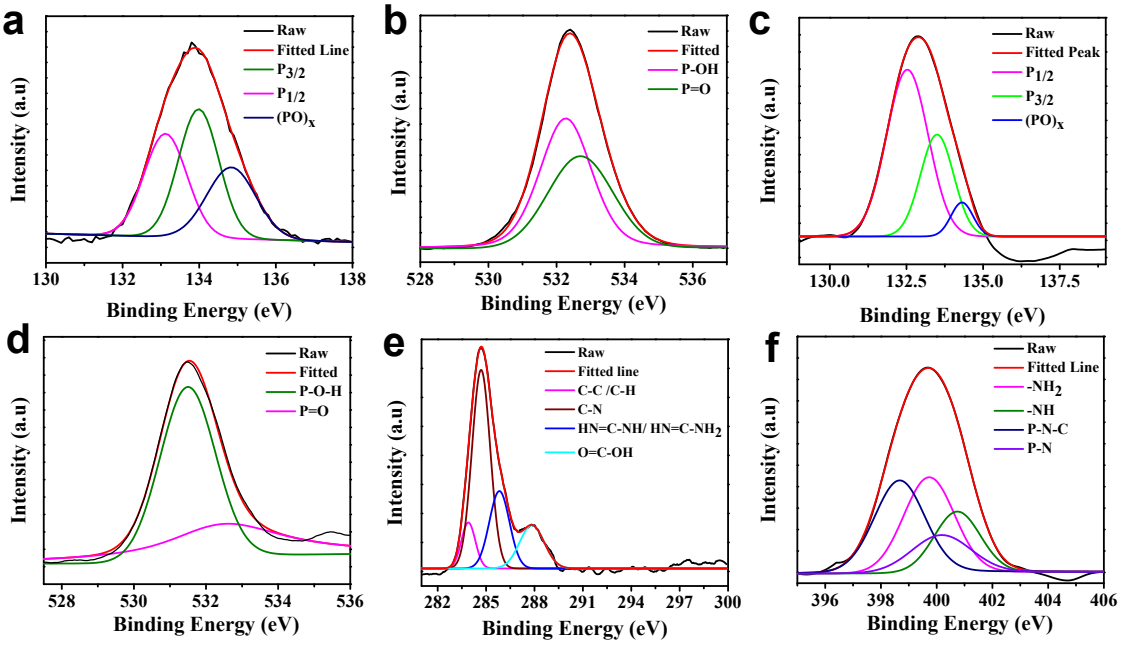

Figure S1. High-resolution XPS spectra of Ph (a) P 2p, & (b) O 1s; high-resolution XPS spectra of PhA composite (c) P 2p, (d) O 1s (e) C 1s & (f) N 1s

An illustrative FESEM image revealed the surface morphologies of the synthesized vermiculite (Vm) clay membrane as shown in Figure S2 (a & b) and PhA incorporated vermiculite clay membrane (Figure 4 (c & d)). It has been observed from the images that Vm has a rough surface. In contrast, the incorporation of PhA nanoparticles on Vm membranes shows deposition of the particles on the surface of the freestanding clay membrane. This signifies the successful fabrication of the nanoparticle-incorporated clay membrane.

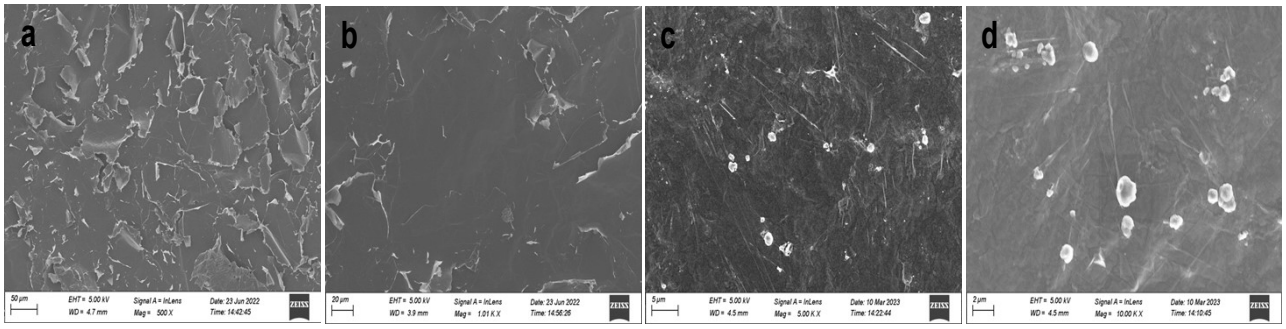

Figure S2. (a) & (b) Show the surface of blank vermiculite clay membrane, and (c) & (d) Show the PhA incorporated vermiculite clay membrane

The following image (Figure S3) shows the probe and probe+analyte under a UV lamp.

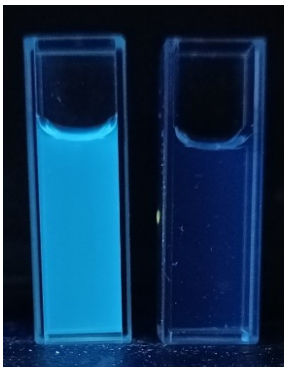

Figure S3. Digital Image of the probe and probe + analyte under UV lamp.

After the successful synthesis of the material, first we analyzed it using UV-visible spectra and fluorescent spectroscopy. PhA exhibits two characteristic peaks in the UV-Vis spectra analysis at 212 nm and 252 nm. This results in the successful synthesis of the PhA composite as shown in Figure 1(a) in the manuscript. The material is highly fluorescent. The digital images corresponding to the material before and after interacting with CSX are in the supplementary file Figure S3. However, upon an increase in the concentration of CSX, the fluorescence intensity gradually decreases. To find out the optimum emission wavelength we have excited the material at different wavelengths and it has been observed that the optimum fluorescence emission wavelength was found to be 358 nm when excited at 300 nm as shown in Figure S4(a). In the case of aqueous media, with an increase in the concentration of the CSX, the fluorescence intensity of the probe decreases as shown the Figure S4(b). The calculated concentrations of the analyte after adding it to the probe which was found to be in the range 1.67 nM- 26.67 nM. To determine the limit of detection (LOD), we have also plotted the calibration curve for the aqueous media as shown in Figure S4(c) by utilizing the following equation-

$$LOD = 3.3 \times RSD/Slope$$

The obtained LOD for aqueous media was found to be about 0.0695 nM for the linear range of 0-80 µL.

We have also calculated the limit quantification (LOQ) using the following equation-

$$LOQ = 10 \times RSD/Slope$$

The determined LOQ value for aqueous media was found to be 0.216 nM.

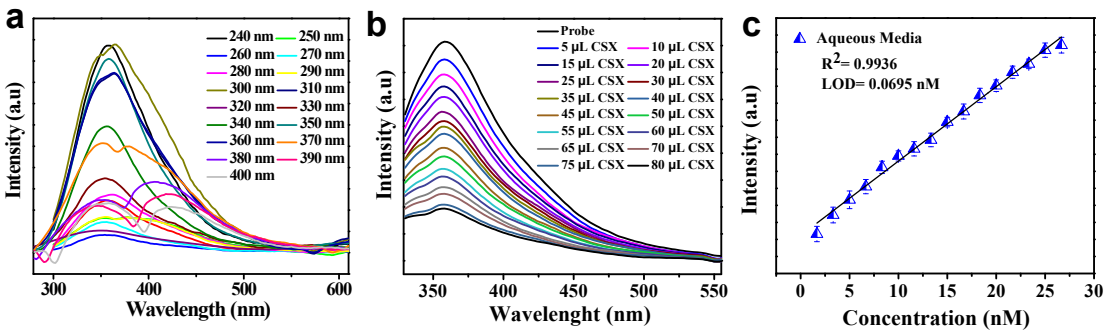

Figure S4. Fluorescence emission spectra of PhA; (b) Quenching efficiency of PhA concerning the concentration of CSX; (c) Calibration plot of turn-off sensing in the concentration range 1.67 nM- 26.67 nM (linear range 0-80 µL)

Figure S5 shows the change in intensity at different pH ranges from 1 to 12 before and after sensing. From the graph, it can be seen that the intensity rises from 1 to 7 with an increase in pH. However, there isn't much of a difference in the pH that can be seen after raising the pH further.

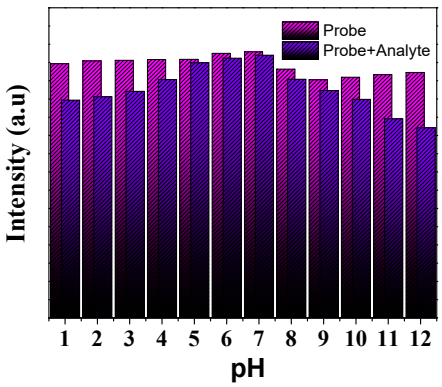

Figure S5. Bar diagram representation of the change in intensity at different pH in the absence and presence of the analyte

Figure S6 shows the effect of temperature on fluorescent intensity with and without the analyte of choice in the temperature range 15-50 ˚C. It has been seen from the calibration graph that there is a change in intensity with an increase in the temperature in the presence as well as the absence of the analyte.

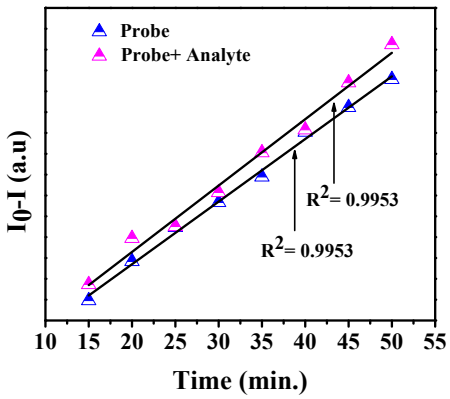

Figure S6. Calibration graph for the change in intensity with an increase in the temperature in the presence and absence of the analyte.

To check the type of quenching, we have analyzed the UV visible spectra of the probe (PhA) with an increase in the concentration of the analyte i.e. CSX as shown in Figure S7. With the increase in the concentration of CSX, there is a disappearance of the peak observed. This means that the probe shows a dynamic quenching at lower concentrations and with an increase in the concentration it starts to form a complex with the analyte. This result can be correlated to the graph obtained from the Stern-Volmer equation where at lower concentrations they follow a linear trend.

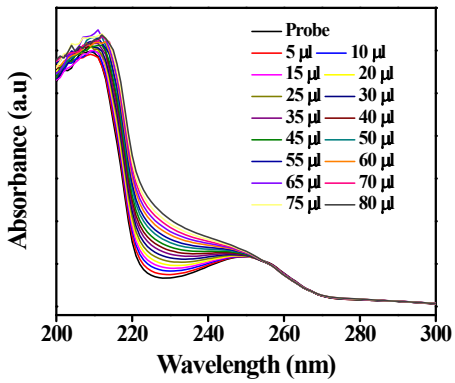

Figure S7. UV visible spectra of PhA with an increase in the concentration of CSX

To distinguish between dynamic and static quenching and to gain a better understanding of the mechanism, a TRPL (time-resolved photoluminescence) examination was carried out. The TRPL spectra of the probe in the presence and absence of an analyte i.e. CSX, are displayed in Figure S8. From the TRPL study, it has been observed that there was not much change in the lifetime in the presence of an analyte, which suggests that there may be dynamic quenching

taking place. The lifetime (χ^2) of the probe was determined to be 2.05 ns, while the lifetime of the analyte was found to be 2.20 ns, favouring dynamic quenching.

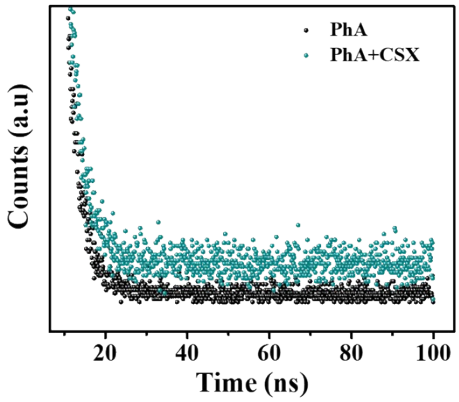

Figure S8. TRPL studies of PhA and PhA + CSX

As shown in Figure S9, we have checked the overlap between the emission and excitation spectra of the probe i.e. the donor with the analyte i.e. acceptor. CSX shows characteristic absorption spectra at 226 nm and 275 nm, which can overlap with the emission and excitation spectra with wavelengths of about 358 nm and 300 nm respectively. This result satisfies the criteria that the fluorophore's emission spectrum must overlap with the analyte absorption spectrum which suggests that IFE may be the cause of quenching.

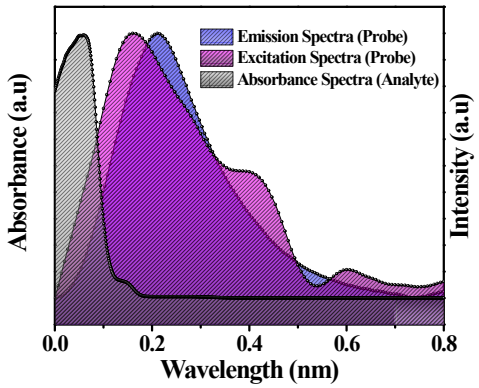

Figure S9. Overlap comparison of absorbance of analyte molecule with the emission and excitation spectra of the probe

As all the criteria satisfy that the fluorophore's emission spectrum must overlap with the analyte absorption spectrum, this means that IFE may be the cause of quenching. The following Scheme S1 in the supplementary file represents the IFE turn-off mechanism.

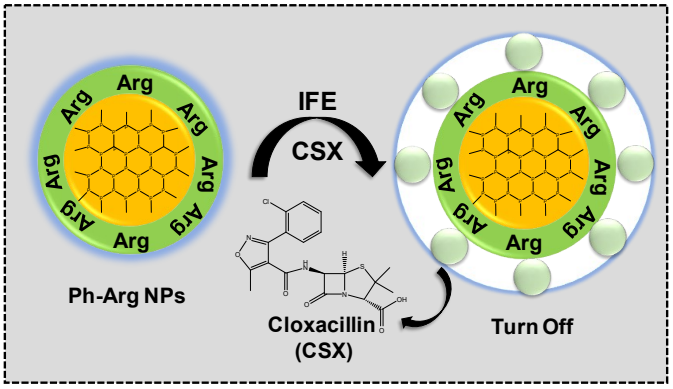

Scheme S1. Schematic representation of the interaction of the probe and probe + analyte

The electrostatic interaction requires close contact between the fluorophore and the analyte so that the transfer of electrons takes place between the two. To confirm the electrostatic interaction, we have measured the zeta potential (ζ) value of Ph, PhA, and PhA + CSX. For Ph, PhA, and PhA + CSX, the observed zeta potential (ζ) values were -27.2 mV, -26.2 mV, and -6.0 mV respectively as shown in Figure S10. After interacting with the CSX, there was a considerable change in the value of the zeta potential, which indicates charge accumulation. As a result, we can infer that the fluorophore and the analyte are interacting electrostatically.

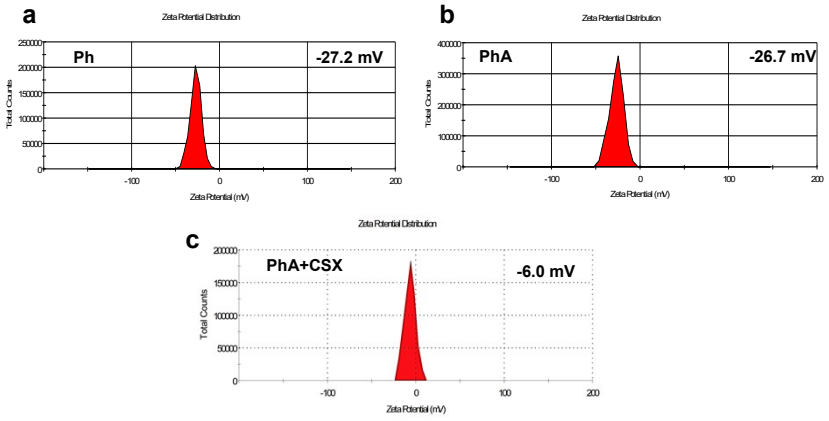

Figure S10. Zeta potential value of (a) Ph; (b) PhA; and (c) PhA + CSX

H-bonding can be used to further validate quenching in addition to IFE and electrostatic interaction. The free -COOH group in CSX has an electron-withdrawing nature. As the intensity of the Ph shifts from 1084 $^{-1}$ to 1093 cm^{-1}, the free -COOH group can easily form H-bonds with the functional groups present in the probe, particularly with the free aliphatic -NH_2 group. Other peaks, as seen in Figure S11, do not exhibit much notable variation in their frequency aside from this.

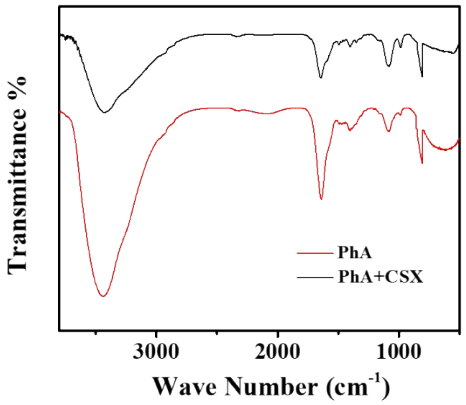

Figure S11. FTIR spectra of PhA and PhA+ CSX

Figure S12 shows the interference study of CSX with some antibiotics, amino acids, and ions that can interfere. Its sensitivity and selectivity towards the chosen analyte, even in the presence of other interfering molecules, is one of the essential qualities of the ideal sensor. We have investigated the selectivity of the probe with several antibiotics such as azaerythromycin (AZAE), biotin, ciprofloxacin hydrochloride hydrate (CPFZ), ceptoperazone sodium (CFZ), ethambutol di hydrochloride (ETB), ivermectin (IVM), monensin sodium salt (MSN), neomycin sulphate (NMS), penicillin sodium salt (PNL) to determine their selectivity towards the sensor. Apart from these antibiotics, we have chosen some other biomolecules such as glycine, alanine, proline, aspartic acid, ascorbic acid, tryptophan, glucose, sucrose, cysteine, and lysine to check the selectivity of the sensor. According to the findings of this investigation, the created sensor system is highly selective for CSX, regardless of other interfering substances including antibiotics and biomolecules.

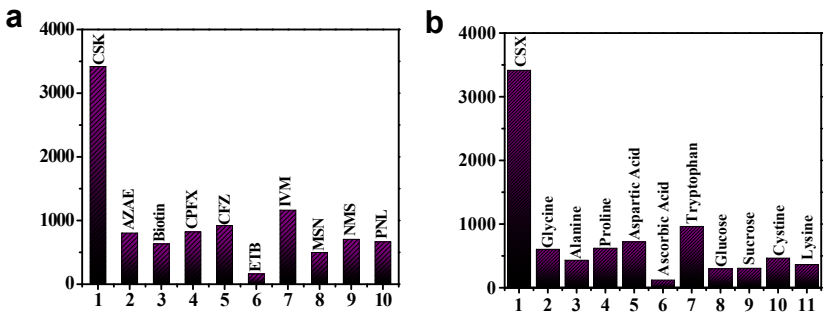

Figure S12. Interference study of CSX with (a) antibiotics; (b) amino acids and ions

We have also calculated the Recover % and RSD mentioned in the following Table S1-

Table S1. Recovery rates of commercially available toned milk pouch and local raw milk spiked with different concentrations of CSX.

Real Samples	*Sl. No.*	*Spiked (μM)*	*Found (μM)*	*Recover (%)*	*RSD*
Commercially available toned milk pouch	1	5	4.802	96	0.030903
	2	10	9.7689	97.69	0.006879
	3	15	14.839	98.93	0.007579
	4	20	20.05	100.25	0.008424
	5	25	24.772	99.09	0.002719
	6	30	30.007	100.02	0.004905
	7	35	34.891	99.69	0.001244
	8	40	39.940	99.85	0.023339
	9	45	45.196	100.44	0.000719
	10	50	49.977	99.95	0.000944
	11	55	55.129	100.23	0.001568
	12	60	59.931	99.89	0.000251
	13	65	65.434	100.67	0.001118
	14	70	70.13	100.19	0.001764
	15	75	74.873	99.83	0.001836
	16	80	79.984	99.98	0.000989
Local raw milk	1	5	5.11	102.2	0.002308
	2	10	10.002	100.02	0.003729
	3	15	15.11	100.73	0.002287
	4	20	20.059	100.29	0.002292
	5	25	25.01	100.04	0.002346
	6	30	29.8832	99.60	0.001944
	7	35	35.118	100.33	0.003027
	8	40	39.23	98.075	0.00119
	9	45	44.79	99.53	0.001036
	10	50	49.17	98.34	0.000349
	11	55	54.51	99.109	0.002211

Figure S13 shows the FTIR spectra of the PhA/Vm membrane before and after exposure to CO_2. Before coming in contact with CO_2 gas molecules, PhA/Vm shows characteristic peaks at 3600-3000 cm^{-1} corresponds to –OH stretching, 1634 cm^{-1}, 1429 cm^{-1} corresponds to P-OH and –COOH bond. The peak observed at 970 cm^{-1} relates to Si-O-Si vibrational stretching of tetrahedral sheets and peaks at 730 cm^{-1}, 667 cm^{-1}, and 515 cm^{-1} can be correlated to the deformation and bending modes of the Si-O bond. After the adsorption of gas molecules, the membranes do not show any significant change. However, a few of the peak positions got changed which may be because of the formation of H-bonding. Apart from this, we have observed three new peaks at 1510 cm^{-1}, 1249 cm^{-1}, and 1183 cm^{-1} which correspond to –NO, -CN, and –CO bond respectively. The following table indicates the changes in peaks observed after chemisorption. The following Table S2 represents the frequencies of PhA/Vm and PhA/Vm+CO_2

Table S2. FTIR frequencies of PhA/Vm and PhA/Vm+CO_2

Materials	**Frequencies**											
PhA/Vm	3558	3418	3283	1634		1429			970	730	667	515
PhA/ Vm+CO_2	3551	3381	3241	1643	1510	1433	1249	1183	952	736	665	507

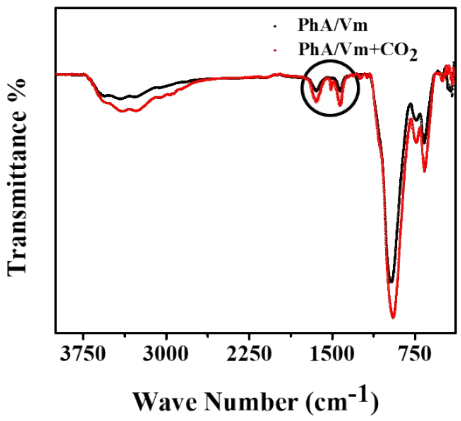

Figure S13. Interference study of CO_2 with volatile organic solvents and acids.

A sensor would be regarded optimal if it is sensitive to and selective for a single analyte. We performed the same experiment with acids and several volatile organic solvents, such as H_2SO_4, HCl, NH_3, acetic acid, acetonitrile, acetone, formaldehyde, methanol, nitromethane, and toluene, to test the effectiveness of the constructed apparatus as shown in Figure S14. The

analysis revealed that the fabricated sensor system, regardless of any obstructing chemicals, is very selective for CO_2.

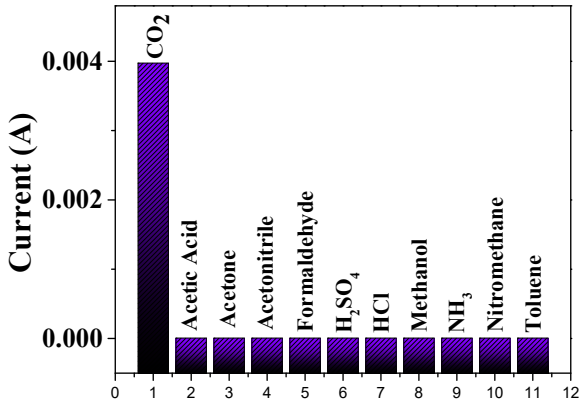

Figure S14. Interference study of CO_2 with volatile organic solvents and acids.